Replication poison treated BRCA1-deficient breast cancers are prone to MRE11 over-resection resulting in single strand DNA accumulation and mitotic catastrophe

Imene Tabet[1], Esin Orhan[1], Ermes Candiello[1#], Lise Fenou[1], Carolina Velazquez[1&], Beatrice Orsetti[1], Geneviève Rodier[1], William Jacot[1,2], Cyril Ribeyre[3], Claude Sardet[1], Charles Theillet[1*]

1- Institut de Recherche en Cancérologie de Montpellier, IRCM U1194, Montpellier University, INSERM, ICM, CNRS, Montpellier, France
2- Clinical Oncology, Institut du Cancer de Montpellier, Montpellier, France
3- Institut de Génétique Humaine, CNRS UMR9002, Montpellier University, Montpellier, France

present address: Candiolo Cancer Institute - FPO – IRCCS, Torino, Italy
& present address: Department of Oncology, KU Leuven and Leuven Cancer Institute (LKI), Leuven, Belgium

* to whom correspondence should be sent charles.theillet@inserm.fr

Abstract

BRCA1, BRCA2 and RAD51 are key players of the homologous recombination (HR) DNA repair pathway, but are also involved in stalled DNA replication fork protection and repair. BRCA1-deficiency is encountered in 25% of Triple Negative Breast Cancer (TNBC). We, thus, tested whether BRCA1-deficient TNBC cell models showed increased sensitivity to replication poisons and in particular to the frequently used RNR inhibitor and a chain terminator gemcitabine. Compared with isogenic BRCA1-proficient cells, gemcitabine treatment of BRCA1-deficient models resulted in large scale replication catastrophe and massive cell death. Cells undergoing replication catastrophe manifested a strong accumulation of single strand DNA (ssDNA), DNA double strand breaks (DSB) and an absence of RPA and/or RAD51 signals. We show here that ssDNA accumulation in BRCA1-deficient cells resulted from uncontrolled MRE11 resection, suggesting that replication fork reversal was a leading response to replication poisoning. Furthermore, we demonstrate that, in addition to replication catastrophe, gemcitabine treated BRCA1-deficient cells are prone to undergo mitotic catastrophe, producing strongly BrdU and γH2AX stained micronuclei (MN) and mitotic bridges. Noticeably these BrdU-positive MN and DNA bridges triggered cGAS activation.

Our data, thus, strongly suggest that gemcitabine treatment could be beneficial in BRCA1-deficient TNBC both in terms of cancer cell death, but possibly as well in terms of antitumor immune response.

Introduction

Homologous recombination deficient (HRD) cancers, originally identified in a subset of ovarian and breast cancers with pathological *BRCA1* or *BRCA2* mutations, are characterized by an elevated genetic instability and increased sensitivity to platinum salts and PARP inhibitors (PARPi) (1). The exquisite sensitivity to treatment of BRCA-deficient tumors has long been considered to result from faulty repair of drug induced double strand DNA breaks (DSB). However, recent data have shown that central HR players such as *BRCA1*, *BRCA2* and *RAD51* play also important roles in the protection, repair and restart of stalled DNA replication forks (2). Moreover, BRCA-deficient models exhibit diminished fork progression speed and accumulate single strand DNA (ssDNA) at replication forks, even in absence of exogenous stress (3), (4) . Altogether, this supports the idea that BRCA-deficient tumors could be at particular risk of undergoing DNA replication malfunction and, thus, be particularly sensitive to replication poison based treatment. DNA replication fork stalling can result from multiple causes, but in case of exposure to anticancer drugs mainly derives from obstacles hindering fork progression or from nucleotide pool imbalance (5). Depending on the number of stalled replication forks and repair capacity, extended replication stress can result in ssDNA accumulation and affect cell viability.

Triple Negative Breast Cancer (TNBC) represent 15% of all breast cancers and its most aggressive subtype. Noticeably, TNBC comprises up to 25% of *BRCA1*-deficient tumors due either to pathological coding mutations or epigenetic silencing of the promoter region (6), (7).

Based on the prevalence of *BRCA1* deficiency in TNBC, we, thus, undertook to study the impact of acute replication stress induced by gemcitabine treatment in BRCA1-deficient models in comparison with their BRCA1-proficients counterparts. We selected gemcitabine, because it is commonly administered in cancer care and functions as a strict replication poison without altering DNA structure. As an irreversible inhibitor of RRM1 it severely affects pyrimidine biosynthesis, but being incorporated in nascent DNA can also act as a chain terminator (8). We show here that, in comparison with their cognate BRCA1-proficient cells, BRCA1-deficient models are superiorly sensitive to gemcitabine and produce a large fraction of cells in replication catastrophe. BRCA1-deficient cells undergoing replication catastrophe were characterized by an accumulation of ssDNA in absence of RPA and/or RAD51 signals, as well as strongly increased DSB. Interestingly, these cells presented an intense pan-nuclear γH2AX staining and their numbers steadily increased with time. Remarkably, accumulation of ssDNA in BRCA1-deficient models undergoing replication catastrophe was dramatically reduced by the MRE11 inhibitor mirin, indicating a leading role of reversed fork nascent DNA resection by MRE11. Furthermore, we demonstrate that BRCA1-deficient cells

undergoing replication catastrophe slipped into mitosis and produced aberrant mitotic figures, in particular strongly BrdU and γH2AX stained micronuclei (MN). Noticeably, these ssDNA loaded MN showed a cGAS immuno-label. Interestingly, γH2AX staining of gemcitabine treated patient derived xenograft (PDX) tumor models revealed that γH2AX levels were increased in gemcitabine sensitive PDX suggesting it could serve as a biomarker for gemcitabine response.

Our data show that BRCA1-deficient cancer cells are prone to undergo lethal ssDNA accumulation when treated with gemcitabine and, thus, suggest that replication poisons could have a favorable therapeutic impact on these tumors.

Materials and methods

Cell lines and CRISPR-Cas9 engineered mutants.

SUM159 TNBC cells were a generous gift from Dr S Ethier (MUSC, Charleston, SC), MDA-MB436, BT549, HCC38 OVCAR8 and UWB1-289 its variant UWB1-289B1 ectopically expressing a full length BRCA1 construct were obtained from ATCC®. The CRISPR-Cas9 BRCA1-KO clone was engineered in house from SUM159PT. SUM-159 were maintained in Ham's F-12 medium (Gibco™, Fisher Scientific, Illkirch-Graffenstaden, France) supplemented with 5% FBS, 10 µg/ml insulin, 1µg/ml hydrocortisone and 1% Antibiotic-antimycotic (100X) (Gibco™, Fisher Scientific, Illkirch-Graffenstaden, France), UWB1.289PT in the 50% RPMI-1640 (Gibco™)/ 50% MEGM (MEGM Bullet Kit; CC-3150, Lonza, Basel, Switzerland) supplemented with 3% FBS, 1% Antibiotic-antimycotic (100X) (Gibco™, Fisher Scientific, Illkirch-Graffenstaden, France), HCC38, BT-549 and OVCAR8 in RPMI-1640 supplemented with 10% FBS and 1% Antibiotic-antimycotic. All cell lines and selected clones were genetically typed by Eurofins Genomics cell line authentification (Eurofins Genomics, Les Ulis, France).

Immunofluorescence

Cells were grown on 12mm diameter slides cover slips in 24 well-plate for 24h, then drugs were added at the IC50 concentration of gemcitabine (Lilly, Fegersheim, France). After 24h drugs were washed off and cells prepared as described below. Cells and tumor sections were sequentially subjected to mild protein pre-extraction (PBS 0.4% Triton, 5min at 4°C), fixation (PBS 4% PFA) and blockage/permeabilization (PBS 3% BSA + 0.2% Triton, 1 hour at room temperature), incubated overnight at 4°C with the primary antibody (diluted in PBS 3% BSA + 0.2% Triton), then with the secondary antibody (diluted in PBS 3% BSA + 0.2% Triton, 1h at room temperature). Between each step, slides were washed 3 times with PBS. Cells were counterstained with DAPI (Fisher Scientific, Illkirch-Graffenstaden, France) to stain the nuclei and cover slips were mounted with MWL4-88 (Citifluor, CliniSciences, Nanterre, France) and stored at 4°C. Antibodies used are described in the Antibody section. Single strand DNA (ssDNA) detection experiments were performed on cells incubated with 10µM BrdU for 24H prior gemcitabine treatment. BrdU was revealed with an antibody in non-denaturing conditions. In MRE11 inhibition experiments cells were incubated in 50µM Mirin (MCE- HY-117693) for 4H prior addition of gemcitabine and Mirin was maintained alongside gemcitabine for: 24H.

Immunofluorescence images were acquired using Zeiss microscope using a 63X-immersion oil lens and generated using Zeiss Blue software. Cells with ≥5 foci in the nucleus were scored using CellProfiler (version 2.2.0, Broad Institute). At least three biological replicates (both vehicle- and olaparib-treated) were analyzed.

For tumor tissues, 6µm cryosections were prepared from OCT embedded deep frozen tissue and mounted on Fisherbrand™ Superfrost™ Plus Microscope Slides (Fisher Scientific, Illkirch-Graffenstaden, France) and stored at -80°C until used. Tumor cryosections were immersed in 0.1% SBB (Sigma Aldrich, Saint Quentin Fallavier, France) and 70% ethanol for 20 minutes at room temperature to reduce tissue autofluorescence and subsequently washed three times for 5 minutes PBS with 0.02% Tween 20. Subsequent immunostaining steps were identical to those applied on cell lines.

Cell cycle determination and replication stress quantification by flow cytometry

Approximately 7 10^5 cells were grown for 24H in 10cm Petri dishes and subjected to a 30 min pulse with 10µM EdU (ThermoFisher Scientific Click-it kit , les Ulis, France) prior gemcitabine treatment for 24H. After drug removal fresh medium was added and cell aliquots were collected at time points 0h, 8h, 24h, 48h. Cells were trypsinated and spun at 1200 rpm for 5min. Cell pellets were resuspended in the pre-extraction solution (PBS + 0.4% Triton) for 5min, then pelleted, fixed with 4%PFA in PBS for 30min at RT and permeabilized in PBS + 1% BSA + 1X saponin for 20min at RT. Cells were sequentially incubated for with the primary and the secondary antibodies for 60 and 30min at RT. Antibodies were diluted in PBS + 1%BSA + 1X saponin. Between primary and secondary antibody incubation cells were washed in PBS+1%BSA. After secondary antibody incubation cells were resuspended in PBS + 1%BSA + 1µg/ml DAPI for DNA counterstaining. FACS analysis was performed using a Gallios Flow instrument (Beckman Coulter, Villepinte, France). Debris and doublets were excluded. Settings were identical in each channel and 10 000 cells were analyzed per aliquot. For the quantification of Sub-G1 fraction applied settings partially excluded debris and doublets. Quantification of apoptosis was done on cell pellets rinsed once in cold PBS and a second time in cold BBA buffer (sterile 0.2 µm HEPES pH7.4, 1.4M NaCl, 25mM CaCl2). Cells were then distributed and resuspended in 50µl BBA buffer + 1µl AnnexinV (Sigma Aldrich, Saint Quentin Fallavier, France) and 0.02µg Propidium Iodide (PI) and incubated at RT for 30min. Then 200 µl PBS were added and cells analyzed.

Cell viability test

Experiments were all performed in 96 well flat bottom plates (Starstedt , , Marnay, France) in which 1500 cells were seeded. After 24H 10µl serial drug dilutions were added in row of 8 wells. This was repeated in triplicates. Cells were exposed to the drug for 24H, gently pelleted and resuspended in fresh medium and left for approximately 2 cell cycle periods (48-56H), before addition of 10µl CCK8 (Cell Counting Kit-8, Tebubio Perray-en-Yvelines, France). Multiwell plates were incubated for 4H at 37°C, solutions in the wells were gently homogenized and 450nM OD was read on a Pherastar photometer (BMG Labtech Champigny-sur-Marne, France). Cell viability (%) = **[(As-Ab) / (Ac-Ab)] ×**

100, where As represents the absorbance of the experimental well, Ab the absorbance of a control well containing medium and CCK8, Ac the absorbance of a control well containing cells, medium and CCK8.

Protein extraction and Western blotting

Protein extracts were prepared by lysing either tumor tissue or cell line pellets on ice for 30 min in 50mM Tris-HCl pH7.4, NaCl 100mM, NaF 50mM, β-glycerophosphate 40mM, EDTA 5mM, Triton X100 1%, Aprotinin 10mg/ml, PMSF 100mM, Leupeptin 1mM, Pepstatin 1mM, followed by a short centrifugation to pellet debris. Protein concentrations were measured using the BCA kit (Fisher Scientific, Illkirch-Graffenstaden, France) SDS-PAGE gel electrophoresis was done on 30µg protein samples subsequently transferred onto nitrocellulose membranes (Amersham, Velizy-Villacoublay, France) and incubated overnight at 4°C with the primary antibody. Antibodies used are listed in a separate section. Membranes were then washed and incubated with the appropriate secondary antibody in 5% non-fat dry milk in PBST for 2h at room temperature and revealed by incubation with Chemiluminescent HRP Substrate (Sigma Aldrich, Saint Quentin Fallavier, France).

Double strand break determination by Pulse Field Gel Electrophoresis (PFGE) of genomic DNA

Pellets of $1x10^6$ treated cells were incorporated in 1% low melting agarose at 50°C and cast into molds (Biorad, Grabels, France) avoiding air bubbles. Samples in agarose plugs were incubated in lysis buffer (100mM EDTA pH8, 0.2% sodium lauryl sarcosine, 1mg/ml proteinase K) for 24H at 37°C, then rinsed 3 times in wash buffer (20mM Tris, 50mM EDTA pH9), then positioned in the wells of a 1% agarose gel in 0.25X TBE. The gel was then run for 24H using pulsed electric field. DNA was labeled using Syber Green and revealed by UV. Fragmented DNA was quantified using the Image lab 6.0.1 software (Biorad, Grabels, France) and normalized relative to the non-fragmented DNA intensity.

PDX models and in vivo treatment

TNBC PDX models establishment was as described [36]. The study was reviewed and approved by the ethics committees for animal experimentations of the University of Montpellier (CEEA-LR-12028). PDX models were established from fresh tumor fragments obtained from the Pathology Department at the Comprehensive Cancer Center of Montpellier (ICM) after informed consent of the patients. Establishment of PDX models was reviewed and approved by the institutional review board. Approximately 50 mm^3 PDX fragments were grafted subcutaneously into the flank of 3-4week old Swiss-nude female mice (Charles Rivers, Saint-Germain-sur-l'Arbresle, France). The present study comprised two experimental arms; vehicle and gemcitabine (Lilly, Fegersheim, France) comprising 8

mice per arm. When median tumor volume reached 100-150mm3, mice were randomly distributed in the two arms and treatment was started. Gemzar was administered was administered by intra-peritoneal (IP) injection twice per week for 4 weeks at 50 mg/kg. At treatment end, mice were euthanized to collect tumor samples for further histological analyses.

Results

BRCA1-deficient cell models exhibit exquisite sensitivity to gemcitabine

We determined the sensitivity to gemcitabine of 4 TNBC and one ovarian cancer cell lines bearing different *BRCA1* statuses; two *BRCA1* wild type (SUM-159 and BT-549), one *BRCA1*-mutated (MDA-MB-436) and two BRCA1 hypermethylated (HCC38 and OVCAR8) (9). MDA-MB-436 and OVCAR8, which showed no BRCA1 protein expression by Western Blot, presented 3 to 10fold lower median inhibitory concentration (IC50) compared with SUM-159, BT-549 and HCC38, which expressed the BRCA1 protein (Fig Sup 1A, C). As all cell lines expressed very similar BRCA2 and RAD51 protein levels, these results suggested a link between the absence of BRCA1 protein expression and increased gemcitabine sensitivity (Supplementary Fig 1C). We engineered a CRISPR *BRCA1*-KO clone from the *BRCA1*-WT SUM-159 cell line, designated hereafter SUM-159B1KO, devoid of BRCA1 protein expression (Supplementary Fig 1C). SUM-159B1KO cells were ten times more sensitive to gemcitabine than the isogenic SUM-159B1WT model (Supplementary Fig 1B). Moreover, gemcitabine treatment increased 5fold the mortality of SUM-159B1KO, in comparison with SUM-159B1WT cells (Figure 1A).

Thereafter, we applied a gemcitabine treatment protocol adapted from that used for IC50 determination, *i.e.* 24H exposure to the drug followed by drug removal and analysis at different time points (Figure 1B). Cell cycle analysis of SUM-159B1WT and SUM-159B1KO cells treated with 150 nM gemcitabine (IC50 of SUM-159B1WT) revealed that while SUM-159B1WT cells reentered cell cycle 48H after removing the drug, SUM-159B1KO further accumulated in S and G2/M cell cycle phases (Supplementary Fig 1D-E).

BRCA1-deficient models exhibit *strongly reduced RAD51 and BRCA2 foci formation upon gemcitabine treatment*

RAD51 and BRCA2 have been shown to play crucial roles in the protection and repair of stalled replication forks (10). We monitored by immunofluorescence nuclear RAD51 and BRCA2 foci formation, in conjunction with that of BRCA1, 53BP1 and FANCD2, in gemcitabine treated SUM-159B1KO and SUM-159B1WT. Compared with SUM-159B1WT, which showed strongly increased BRCA1, BRCA2 and RAD51 foci formation, peaking at 8H and slowly receding at 24 and 48H, BRCA1, BRCA2 and RAD51 foci were impaired in SUM-159B1KO, whereas 53BP1 and FANCD2 foci strongly increased (Figure 1C-F). We made very similar observations in the *BRCA1* mutated UWB1.289 ovarian carcinoma cell line compared with its ectopically expressing *BRCA1* UWB1.289B1 variant and observed impaired BRCA2 and RAD51 associated with increased FANCD2 and 53BP1 foci formation in parental UWB1.289 cells (Supplementary Fig 1F-G).

Gemcitabine treated BRCA1-deficient models undergo persistent replicative stress

Cell populations subjected to replication stress exhibit an increase of γH2AX-positive and RPA-positive cell numbers, but in case of severe replication stress γH2AX-positive cells outnumber RPA-positive cells (11). We performed a time course FACS analysis of γH2AX-positive and RPA-positive cells in gemcitabine treated SUM-159B1WT and SUM-159B1KO and noted a temporary imbalance of the γH2AX/RPA ratio at 0H and 8H in SUM-159B1WT (Figure 2A), whereas SUM-159B1KO exhibited a strong and persisting γH2AX/RPA imbalance (Figure 2B). The excess of γH2AX-positive relative to RPA-positive cells in gemcitabine treated SUM-159B1KO in comparison with SUM-159B1WT was also shown in immunofluorescence analyses (Figure 2C-F). While the number of γH2AX-positive SUM-159B1KO cells remained stable between 24H and 48H, the fraction of RPA-positive steadily decreased between 8H and 48H (Figure 2F). In identical conditions, SUM-159B1WT showed no imbalance between γH2AX-positive and RPA-positive cells, with decreasing numbers of γH2AX-positive and/or RPA-positive cells at 48H (Figure 2E). Similar observations were made in UWB1.289 and UWB1.289B1 cells, where *BRCA1*-deficient UWB1.289 cells showed a strong imbalance between γH2AX-positive and RPA-positive cells, while BRCA1-proficient models did not (Supplementary Fig 2A-D). These data, thus, supported that BRCA1-deficiency was associated with strongly increased and persistent replication stress upon gemcitabine treatment.

BRCA1-deficient cells are prone to replication catastrophe, accumulate large quantities of ssDNA, show pan-nuclear γH2AX-staining and no RPA signal.

A large fraction of gemcitabine treated SUM-159B1KO cells presented a strong accumulation of ssDNA revealed by intense non-denaturing BrdU immunostaining (Figure 3A-B). We noted that strongly BrdU-staining was concomitant to the absence of RPA signal in SUM-159B1KO cells, a situation indicative of replication catastrophe. BrdU-positive/RPA- negative cells accumulated over time reaching up to 70% of the population at 48H (Figure 3B-D). Constrastingly, in SUM-159B1WT BrdU-positive/RPA-negative cells peaked at 20% (Figure 3C). Noticeably, cells with intense BrdU-staining and no RPA signal presented strong pan-nuclear γH2AX-staining (Figure 3E-G-H). By contrast, cells showing γH2AX foci were RPA-positive (Figure 3G-H). Furthermore, the number of pan-nuclear γH2AX staining cells increased over time in SUM-159B1KO and other BRCA1-deficient cell models, reaching up to 80% of the BrdU-positive cells 48h after drug removal (Figure 3F, Supplementary Fig 3A-C). It was also of note that a large majority of pan-nuclear γH2AX staining SUM-159B1KO cells showed no RAD51 foci (γH2AX-positive/RAD51-negative) and, contrastingly, presented increased numbers of 53BP1 and FANCD2 foci in comparison with SUM-159B1WT (Figure 4A-B-C-D-E-F). These data, thus, indicated that BRCA1-deficient cells undergoing replication catastrophe were characterized by an intense pan-nuclear γH2AX staining associated with a joint absence of RPA and RAD51 signals and a strong recruitment of 53BP1 and FANCD2.

MRE11 inhibition strongly reduced ssDNA accumulation and DSB levels in gemcitabine treated SUM 159-B1KO *cells*

We wondered if the strong increase of ssDNA in gemcitabine treated BRCA1-deficient models was due to nascent strand resection by the MRE11 exonuclease in the absence of RAD51 (10). However, the absence of RPA, RAD51 and BRCA2 in *SUM 159*-B1KO cells undergoing replication catastrophe suggested a context favorable to uncontrolled MRE11 resection. To verify this hypothesis, we treated SUM-159B1KO and SUM-159B1WT models with 150 nM gemcitabine +/- 50 µM of the MRE11-inhibitor mirin. Noticeably, MRE11-inhibition strongly reduced the number of BrdU-positive and γH2AX pan-nuclear staining cells in SUM-159B1KO, compared with a minor effect in SUM-159B1WT (Figure 5A-H).

Furthermore, as unresolved replication fork stalling can result in fork breakdown and produce double strand DNA breaks (DSB), we determined DSB levels in gemcitabine treated SUM-159B1WT and SUM-159B1KO by pulse field gel electrophoresis (PFGE). Gemcitabine treated SUM-159B1KO accumulated at least 50% more DSB in comparison with SUM-159B1WT in identical conditions. Noticeably, addition of mirin reduced by 85% the level of DSB in gemcitabine treated SUM-159B1KO, compared with SUM-159WT where reduction was of 20% (Figure 5I). These results were in line with the effect of mirin on ssDNA accumulation (Figure 5B, F). However, it has also been proposed, that, in BRCA2-defective models submitted to replication stress, DNA breaks resulted from apoptotic DNA fragmentation, rather than from replication fork breakdown (12). We, therefore, verified the impact of ZVAD-FMK, a pan-caspase inhibitor, on DSB levels and observed no reduction in gemcitabine treated SUM-159B1KO and SUM-159B1WT, despite a strong reduction of apoptic cell numbers (Figure 5K, Supplementary Fig 4A). Hence, our data indicated that uncontrolled MRE11 resection played a major role in the accumulation of ssDNA in gemcitabine treated BRCA1-deficient models and was associated with a severe increase of DSBs observed.

SUM-159B1KO cells undergoing replication catastrophe slip into mitosis and produce mitotic catastrophe.

As we determined that gemcitabine treated BRCA1-deficient cells tended to accumulate in G2/M (Figure 1E) and formed micronuclei (MN), we asked whether this resulted from mitotic slippage and catastrophic mitoses. To ascertain mitotic slippage, we synchronized the cells in G1 by exposing them to 100nM of the CDK4/6 inhibitor palbociclib for 24H. Cells reached S phase synchronously 8h after palbociclib removal, time at which we added 1µM gemcitabine for 3H (Supplementary Fig 5A, B). FACS monitoring of cell cycle progression revealed that SUM-159B1KO accumulated in M phase 72H and 96H after removing gemcitabine. By contrast, SUM-159B1WT resumed cell cycle at 96H (Figure 6A,B). We noted that the cell cycle profile of gemcitabine treated SUM-159B1KO was similar to that

of cells treated with a combination of 50nM gemcitabine + 50nM of the CHK1 inhibitor PF-0477736 (Supplementary Fig 5C,D), suggesting that the G2 to M checkpoint in SUM-159B1KO cells was defective. Unscheduled progression into mitosis was in line with the large fraction of aberrant mitoses (multipolar divisions, ultrafine mitotic bridges or MN), representing up to 70% of the mitotic figures observed in gemcitabine treated SUM-159B1KO cells. In comparison, aberrant mitoses represented only 20% in SUM-159B1WT (Figure 6C, D, Supplementary Fig 5F, G).

50% micronuclei in SUM-159B1KO are linked to replicative catastrophe and sensed by cGAS

MN are linked to lagging mitotic chromosomes due to non-resolved genomic damage {Flynn:jq}. Remarkably, we noted that MN in SUM-159B1KO presented both pan-nuclear γH2AX and strong BrdU staining, indicating they encompassed long stretches of ssDNA (Figure 6E). Due to the observed impact of MRE11 inhibition on ssDNA accumulation in SUM-159B1KO, we tested whether mirin affected MN formation and noted that MN numbers were reduced by 53% in mirin treated SUM-159B1KO. In comparison, mirin treatment reduced MN by only 17% in SUM-159B1WT (Figure 6F-G). Because MN could also be associated with apoptotic nuclear fragmentation, we tested the impact of ZVAD-FMK on MN formation in gemcitabine treated SUM-159B1WT and SUM-159B1KO models. The reduction of MN numbers by ZVAD-FMK was of 70% in SUM-159B1WT and 50% in SUM-159B1KO (Figure 6I-J). These data, thus, suggested that 80% MN resulted from apoptotic fragmentation in SUM-159B1WT cells, while in SUM-159B1KO over 50% MN resulted from mitotic catastrophe, the rest being linked to apoptosis.

It has been reported that mitotic bridges and MN could activate the cyclic GMP-AMP synthase (cGAS) sensing response, due to cytoplasmic exposure of DNA {Flynn:jq},(13). We noted that, in gemcitabine treated SUM159B1KO, ultrafine DNA bridges and up to 30% BrdU-positive micronuclei showed a clear cGAS signal, compared with 10% cGAS positive MN in SUM159B1WT (Figure 6J-K, Supplementary Fig 5H).

Our data, thus, indicate that BRCA1-deficient cells undergoing replication catastrophe slip into mitosis resulting in MN production that trigger cGAS.

Gemcitabine responsive TNBC PDX models show increased γH2AX and cGAS staining

Based on cell culture model data, we verified whether increased γH2AX staining levels could be related to gemcitabine responsiveness of breast cancer patient derived xenograft (PDX) models. To this mean, we determined the response of three TNBC PDXs to two 50mg/kg weekly injections of gemcitabine for four weeks (Supplementary Fig 6A-C). Post-treatment residual tumors were sampled after the last drug injection for immunostaining purposes. γH2AX and cGAS immunolabeling, performed on gemcitabine and mock treated tumor sections, showed that the number of γH2AX-positive cells were highest in PDX b4122 which responded best to gemcitabine and lowest in PDX

15b0018 that progressed under treatment. PDX b3804, which was stabilized under gemcitabine treatment, presented intermediate numbers of γH2AX staining levels (Supplementary Fig 6D-E).

Discussion

The data presented here show that *BRCA1*-deficient TNBC cell models treated with gemcitabine were prone to replication catastrophe and suffered from massive cell death, in contrast with their *BRCA1*-proficient counterpart in which replicative stress was transient and resulted in modest mortality. Replication catastrophe has been defined as the result of an acute production of ssDNA and exhaustion of the RPA protein pool in the cell. It was manifested by a strong accumulation of BrdU-positive/RPA-negative cells in gemcitabine treated BRCA1-deficient models (11). However, the RPA titration does not, by itself, explain why replication catastrophe is aggravated in a *BRCA1*-deficient context. We noted that the MRE11 inhibitor mirin induced a strong decrease of ssDNA accumulation in gemcitabine treated *BRCA1*-deficient models, while showing little effect in isogenic *BRCA1*-proficient cells. Hence, we conclude that uncontrolled MRE11 exonuclease resection played a major role in the massive ssDNA accumulation observed in BRCA1-deficient models. MRE11, a 3' to 5' exonuclease essential in DSB HR repair, has also been associated with reversed fork repair, where it is recruited onto the nascent DNA strand by CtIP (14). However, fork reversal, a remodeling process proposed to put stalled replication forks on hold to allow repair, creates structures that are vulnerable to nucleolytic attack. This is especially the case in a BRCA-deficient context, where RAD51 recruitment is low or absent (10), (15), (16), (17), (14). Uncontrolled MRE11 resection in our gemcitabine treated BRCA1-deficient models was, thus, in line with the absence of RAD51 foci in BrdU-positive/RPA-negative cells. It was of note that contrarily to RAD51, recruitments of 53BP1 and FANCD2 were increased in gemcitabine treated BRCA1-deficient cells, but with no apparent effect on fork protection. Yet, it must be noted that MRE11 is not processive enough to explain the massive ssDNA accumulation observed in BRCA1-deficient models and Lemaçon and coworkers (14) have shown that production of long ssDNA stretches necessitated the combined activity of EXO1 nuclease. Furthermore, MRE11 fork resection has been shown to be tightly linked with fork reversal (18). Hence, our data strongly suggest that fork reversal played a major part in the response to gemcitabine treatment in our conditions (19), (14), (20). DNA synthesis repriming, by way of the primase directed DNA polymerase PRIMPOL, is an alternative response to fork reversal (2). Repriming by PRIMPOL occurs downstream of stalled forks and leaves ssDNA gaps that are primarily filled by TLS polymerases. Furthermore, MRE11 plays no documented role in the repriming and ssDNA gaps formation process (21) (2). Noticeably, it has been proposed that ssDNA accumulation in BRCA-deficient models submitted to replication stress resulted from ssDNA gaps and unscheduled DNA synthesis, while MRE11 resection had little impact in the process (12). Data presented in this work, thus, dispute this assertion. It is of note that Panzarino and coworkers mainly based their observations on olaparib treatment and PARPi have been shown to repress fork reversal and activate

repriming thus favoring ssDNA gap formation (2). In line with the link between PARPi and repriming, it has been shown that the number of ssDNA gaps increased in proportion with olaparib concentrations (22). It has also been shown that repriming could be activated in conditions of mild nucleotide pool depletion, whereas elevated doses and prolonged exposure would preferentially result in fork reversal (20).

Remarkably, BRCA1-deficient cells undergoing replication catastrophe instead of showing γH2AX foci were characterized by an intense pan-nuclear γH2AX staining pattern and that their numbers increased 3fold between 24 and 48H after drug removal. By contrast, BrdU-positive cells numbers increased regularly between 8 and 24H. This suggested that pan-nuclear γH2AX staining could represent late, possibly final, stages of replication catastrophe. Moeglin and coauthors (23) proposed that pan-nuclear γH2AX could be a pre-apoptotic signal, however, our results show that the apoptosis inhibitor ZVAD-FMK had little impact on pan-nuclear γH2AX staining cell numbers. We, thus, favor the hypothesis that pan-nuclear γH2AX signal is triggered by massive DSB resulting from replication fork breakdown during late stages of replicative catastrophe, thus explaining the shift from foci to pan-nuclear staining. We, then, questioned whether the level of γH2AX staining could reflect the sensitivity to gemcitabine in treated TNBC. γH2AX immunostaining performed on a series of gemcitabine treated TNBC PDXs, indeed, suggested that γH2AX levels were increased, both in terms of positive cell numbers, but also staining intensity in PDX models showing better treatment response.

Somewhat to our surprise, BRCA1-deficient TNBC cells suffering from replication catastrophe, despite robust ssDNA accumulation, reached M phase and produced aberrant mitoses, particularly, strongly BrdU labeled micronuclei (MN). Since MRE11 inhibition reduced BrdU-positive MN numbers, it appears most likely that BrdU-positive MN originated from lagging chromosomes bearing long stretches of ssDNA (24). The presence, in the aberrant mitotic fields of gemcitabine treated SUM159-B1KO cells, of fine chromatin bridges, supported this hypothesis. In addition we noted that BrdU and γH2AX labeled MN also presented a strong cGAS signal. Cyclic GMP–AMP synthase (cGAS) is a cytoplasmic DNA sensor and component of the innate immune system that triggers antibacterial or antiviral inflammatory response (25). cGAS is also frequently activated in tumor cells and has been shown to react with MN, despite the presence of the nuclear envelope (13). But based on the link between chromatin bridges and MN, it has also been proposed that cGAS in MN could result from mitotic bridges sensing prior MN formation and nuclear envelope reconstitution {Flynn:jq}. DNA recognition by cGAS is an early signal of the interferon inflammatory immune response, which in cancer could trigger an antitumor immune response, especially as cGAMP has been shown to participate to paracrine spread and activate cells from the microenvironment {Flynn:jq}.

Hence, our data suggest that gemcitabine treatment of BRCA-deficient TNBC could be beneficial to patients because of; (1) its impact on tumor cell survival, (2) the induction of a secondary antitumor immune response.

Conflict of interest:
None of the authors has a conflict of interest to disclose

Author contribution
Imene Tabet; Conceptualization, investigation, validation, methodology, drafting and editing the paper. Esin Orhan; investigation, validation, methodology, editing the draft. Ermes Candiello; Conceptualization, investigation, editing the draft. Carolina Velazquez; investigation, data curation, validation, methodology. Lise Fenou; resources, validation, data curation, methodology. Beatrice Orsetti; methodology, resources. Geneviève Rodier; methodology, validation, editing the draft. William Jacot; resources, editing the draft. Cyril Ribeyre; investigation, data curation, validation, methodology, editing the draft. Claude Sardet; funding acquisition, supervision, editing the draft. Charles Theillet; Conceptualization, Supervision and coordination, writing and editing the paper, funding acquisition,

Ethics approval
Patients whose tumor was used to generate PDX signed informed consent and the preclinical assay was reviewed and approved by the ethics committees for animal experimentations of the University of Montpellier (CEEA-LR-12028) and received the approval number 25612.

Data availability
The data presented in this study are available on reasonable request from the corresponding author.

Acknowledgements
The authors sincerely acknowledge Dr Philippe Pasero (IGH) and Dr Isabelle Jariel (IRCM) helpful comments during the course of this work and constructive comments on the manuscript. Furthermore, sincere thanks are due to the staffs of the animal facility at IRCM for their constant support and expert help.

Grants and financial support
This work benefited from the following financial support: Astra-Zeneca contract # 2018-02069, Institut National du Cancer PRTK-2017 MODUREPOIS, Ligue Nationale Contre le Cancer 'Comité régional Occitanie-Est' 2021-R22031FF and the SIRIC Montpellier Cancer Grant INCa-DGOS-Inserm_12553.

Author information
Ermes Candielo, present address; Candiolo Cancer Institute - FPO – IRCCS, 10060 Candiolo (TO)-Italy
Carolina Velazquez, present address; Gynecological Oncology Laboratory, Department of Oncology, KU Leuven and Leuven Cancer Institute (LKI), 3000 Leuven, Belgium.

References

1. Lord CJ, Ashworth A. BRCAness revisited. Nature Publishing Group. 2016 Feb;16(2):110–20.

2. Quinet A, Tirman S, Jackson J, Šviković S, Lemaçon D, Carvajal-Maldonado D, et al. PRIMPOL-Mediated Adaptive Response Suppresses Replication Fork Reversal in BRCA-Deficient Cells. Molecular Cell. 2020 Feb 6;77(3):461–9.

3. Daboussi F, Courbet S, Benhamou S, Kannouche P, Zdzienicka MZ, Debatisse M, et al. A homologous recombination defect affects replication-fork progression in mammalian cells.

Journal of Cell Science. 2008 Jan;121(Pt 2):162–6.

4. Wilhelm T, Ragu S, Magdalou I, Machon C, Dardillac E, Técher H, et al. Slow Replication Fork Velocity of Homologous Recombination-Defective Cells Results from Endogenous Oxidative Stress. Maizels N, editor. 2016 May 2;12(5):e1006007–20.

5. Zeman MK, Cimprich KA. Causes and consequences of replication stress. Nat Cell Biol. 2014 Jan;16(1):2–9.

6. Couch FJ, Hart SN, Sharma P, Toland AE, Wang X, Miron P, et al. Inherited Mutations in 17 Breast Cancer Susceptibility Genes Among a Large Triple-Negative Breast Cancer Cohort Unselected for Family History of Breast Cancer. Journal of Clinical Oncology. 2015 Jan 29;33(4):304–11.

7. Jacot W, Lopez-Crapez E, Mollevi C, Boissière-Michot F, Simony-Lafontaine J, Ho-Pun-Cheung A, et al. BRCA1 Promoter Hypermethylation is Associated with Good Prognosis and Chemosensitivity in Triple-Negative Breast Cancer. Cancers (Basel). 2020 Mar 30;12(4).

8. Hawryłkiewicz A, Ptaszyńska N. Gemcitabine Peptide-Based Conjugates and Their Application in Targeted Tumor Therapy. Molecules. 2021 Jan;26(2).

9. Elstrodt F, Hollestelle A, Nagel JHA, Gorin M, Wasielewski M, van den Ouweland A, et al. BRCA1 mutation analysis of 41 human breast cancer cell lines reveals three new deleterious mutants. Cancer Res. 2006 Jan;66(1):41–5.

10. Hashimoto Y, Ray Chaudhuri A, Lopes M, Costanzo V. Rad51 protects nascent DNA from Mre11-dependent degradation and promotes continuous DNA synthesis. Nat Struct Mol Biol. 2010 Nov;17(11):1305–11.

11. Toledo LI, Altmeyer M, Rask M-B, Lukas C, Larsen DH, Povlsen LK, et al. ATR prohibits replication catastrophe by preventing global exhaustion of RPA. Cell. 2013 Nov 21;155(5):1088–103.

12. Panzarino NJ, Krais JJ, Cong K, Peng M, Mosqueda M, Nayak SU, et al. Replication Gaps Underlie BRCA Deficiency and Therapy Response. Cancer Res. 2021 Mar 1;81(5):1388–97.

13. Mackenzie KJ, Carroll P, Martin C-A, Murina O, Fluteau A, Simpson DJ, et al. cGAS surveillance of micronuclei links genome instability to innate immunity. Nature. 2017 Aug 24;548(7668):461–5.

14. Lemaçon D, Jackson J, Quinet A, Brickner JR, Li S, Yazinski S, et al. MRE11 and EXO1 nucleases degrade reversed forks and elicit MUS81-dependent fork rescue in BRCA2-deficient cells. Nat Comms. 2017 Oct 16;8(1):860.

15. Schlacher K, Christ N, Siaud N, Egashira A, Wu H, Jasin M. Double-Strand Break Repair-Independent Role for BRCA2 in Blocking Stalled Replication Fork Degradation by MRE11. Cell. 2011 May;145(4):529–42.

16. Thangavel S, Berti M, Levikova M, Pinto C, Gomathinayagam S, Vujanovic M, et al. DNA2 drives processing and restart of reversed replication forks in human cells. J Cell Biol. 2015 Mar;208(5):545–62.

17. Mijic S, Zellweger R, Chappidi N, Berti M, Jacobs K, Mutreja K, et al. Replication fork reversal

triggers fork degradation in BRCA2-defective cells. Nat Comms. 2017 Oct 16;8(1):859.

18. Berti M, Cortez D, Lopes M. The plasticity of DNA replication forks in response to clinically relevant genotoxic stress. Nat Rev Mol Cell Biol. 2020 Oct;21(10):633–51.

19. Zellweger R, Dalcher D, Mutreja K, Berti M, Schmid JA, Herrador R, et al. Rad51-mediated replication fork reversal is a global response to genotoxic treatments in human cells. J Cell Biol. 2015 Mar 2;208(5):563–79.

20. Quinet A, Tirman S, Cybulla E, Meroni A, Vindigni A. To skip or not to skip: choosing repriming to tolerate DNA damage. Molecular Cell. 2021 Feb 18;81(4):649–58.

21. Guilliam TA, Doherty AJ. PrimPol-Prime Time to Reprime. Genes (Basel). 2017 Jan;8(1).

22. Cong K, Peng M, Kousholt AN, Lee WTC, Lee S, Nayak S, et al. Replication gaps are a key determinant of PARP inhibitor synthetic lethality with BRCA deficiency. Molecular Cell. 2021 Aug 5;81(15):3128–3144.e7.

23. Moeglin E, Desplancq D, Conic S, Oulad-Abdelghani M, Stoessel A, Chiper M, et al. Uniform Widespread Nuclear Phosphorylation of Histone H2AX Is an Indicator of Lethal DNA Replication Stress. Cancers (Basel). 2019 Mar;11(3):355–22.

24. Hoffelder DR, Luo L, Burke NA, Watkins SC, Gollin SM, Saunders WS. Resolution of anaphase bridges in cancer cells. Chromosoma. 2004 Jun;112(8):389–97.

25. Motwani M, Pesiridis S, Fitzgerald KA. DNA sensing by the cGAS-STING pathway in health and disease. Nat Rev Genet. 2019 Nov;20(11):657–74.

Figure Legends

Figure 1: BRCA1-deficiency is associated with accrued gemcitabine mortality and absence of HR response A: mortality graphs of gemcitabine treated SUM159B1WT (black) and SUM159B1KO (red) cells. Cell death was assessed by FACS quantification and combines AnnexinV+ and propidium iodide+ cells. **B:** treatment protocol applied here; cells were exposed to the drug for 24h, then left to recover in fresh medium for 48h before mortality was measured. **C, D:** immunofluorescence analysis and quantification of BRCA1, BRCA2, RAD51 and 53BP1 nuclear foci formation in SUM-159B1WT cells upon gemcitabine treatment. **E, F:** same as C, D but with SUM-159B1KO cells. Cells presenting more than 10 nuclear foci by immunofluorescence were scored positive and at least 300 cells were scored per slide.

Figure 2: Gemcitabine treatment induces severe and persitent replication stress in BRCA1-deficient cell models. A, B: FACS analysis quantification of γH2AX-positive and RPA-positive cell fractions in SUM-159B1 (A) and SUM-159B1KO (B), note the imbalance between γH2AX and RPA**. C, D:** the γH2AX/RPA imbalance was also noticeable by immunofluorescence. selected sets of immunofluorescence sections of SUM-159B1WT (C) and SUM-159B1KO (D) stained with anti-γH2AX (red) and RPA (green) antibodies **E, F:** quantification of γH2AX-positive and RPA-positive cells by IF, at least 300 cells were scored by slide.

Figure 3: cells undergoing replication catastrophe are characterized by an intense BrdU, absence of RPA signal and pan-nuclear γH2AX staining. A, B: examples and quantification of RPA and BrdU immunofluorescence staining in SUM-159B1WT and SUM-159B1KO. Yellow circles in B indicate cells showing no RPA signal and intense BrdU staining **C, D:** γH2AX, BrdU and RPA32 staining patterns 48h after drug removal in SUM-159B1WT and SUM-159B1KO. Yellow circles in D indicate cells showing no or low RPA signal and a strong pan-nuclear γH2AX staining**. E:** quantification of the fraction of BrdU+ cells with pan-nuclear γH2AX staining in SUM-159B1WT and SUM-159B1KO**. F**: quantification of the fraction of pan-nuclear γH2AX staining cells showing no RPA32 signal in SUM-159B1WT and SUM-159B1KO.

Figure 4: cells with pan-nuclear γH2AX staining show no RAD51 foci, but strong 53BP1 and FANCD2 signals. A, B: examples of γH2AX and RAD51 immunofluorescence staining 48H after drug removal and quantification of pan-nuclear γH2AX+/RAD51- cells in SUM-159B1WT and SUM-159B1KO l. **C, D:** examples of γH2AX and 53BP1 immunostaining and quantification of pan-nuclear γH2AX+/53BP1+ cells in SUM-159B1WT and SUM-159B1KO. **E, F:** examples of γH2AX and FANCD2 immunostaining and quantification of pan-nuclear γH2AX+/FANCD2+ cells in SUM-159B1WT and SUM-159B1KO

Figure 5: MRE11 is instrumental for ssDNA accumulation and onset of replication catastrophe in gemcitabine treated BRCA1-deficient cells. A, B, C, D: impact of Mirin treatment on the number of BrdU and γH2AX positive cells in gemcitabine treated SUM-159B1WT. γH2AX and BrdU immunofluorescence staining in cells treated with Gemcitabine (top row) and Gemcitabine + mirin (bottom row) (A). Quantification of BrdU+ cells in the different conditions (B). Quantification of γH2AX+ cells (C). Quantification of cells with pan-nuclear γH2AX staining (D). **E, F, G, H**: impact of Mirin treatment on the number of BrdU and γH2AX positive cells in gemcitabine treated SUM-159B1KO. γH2AX and BrdU immunofluorescence staining in cells treated with Gemcitabine (top row) and Gemcitabine + mirin (bottom row) (E). Quantification of BrdU+ cells in the different conditions (F). Quantification of γH2AX+ cells (G). Quantification of cells with pan-nuclear γH2AX staining (H). **I:** quantification of DSB breaks in SUM-159B1WT (black bars) and SUM-159B1KO (red bars) treated with gemcitabine +/- mirin. **J**: quantification of DSB breaks in SUM-159B1WT and SUM-159B1KO treated with gemcitabine +/- Z-VAD.

Figure 6: replication catastrophe BRCA1-deficient cells produce aberrant mitoses and trigger cGAS-STING response. A, B: cell cycle changes in synchronized SUM-159B1WT and SUM-159KO cells. Results present the ratio Treated/Nontreated cells. **C:** fraction of aberrant mitoses in gemcitabine treated cells. Red SUM-159B1KO, black SUM-159B1WT. **D:** micronuclei formation in gemcitabine treated SUM-159B1WT and SUM-159KO cells. **E**: in SUM-159KO micronuclei are BrdU and γH2AX positive. **F, G:** impact of mirin treatment on micronuclei numbers**. H, I:** impact of Z-VADFMK treatment on micronuclei numbers. **J, K:** γH2AX+ micronuclei show cGAS staining.

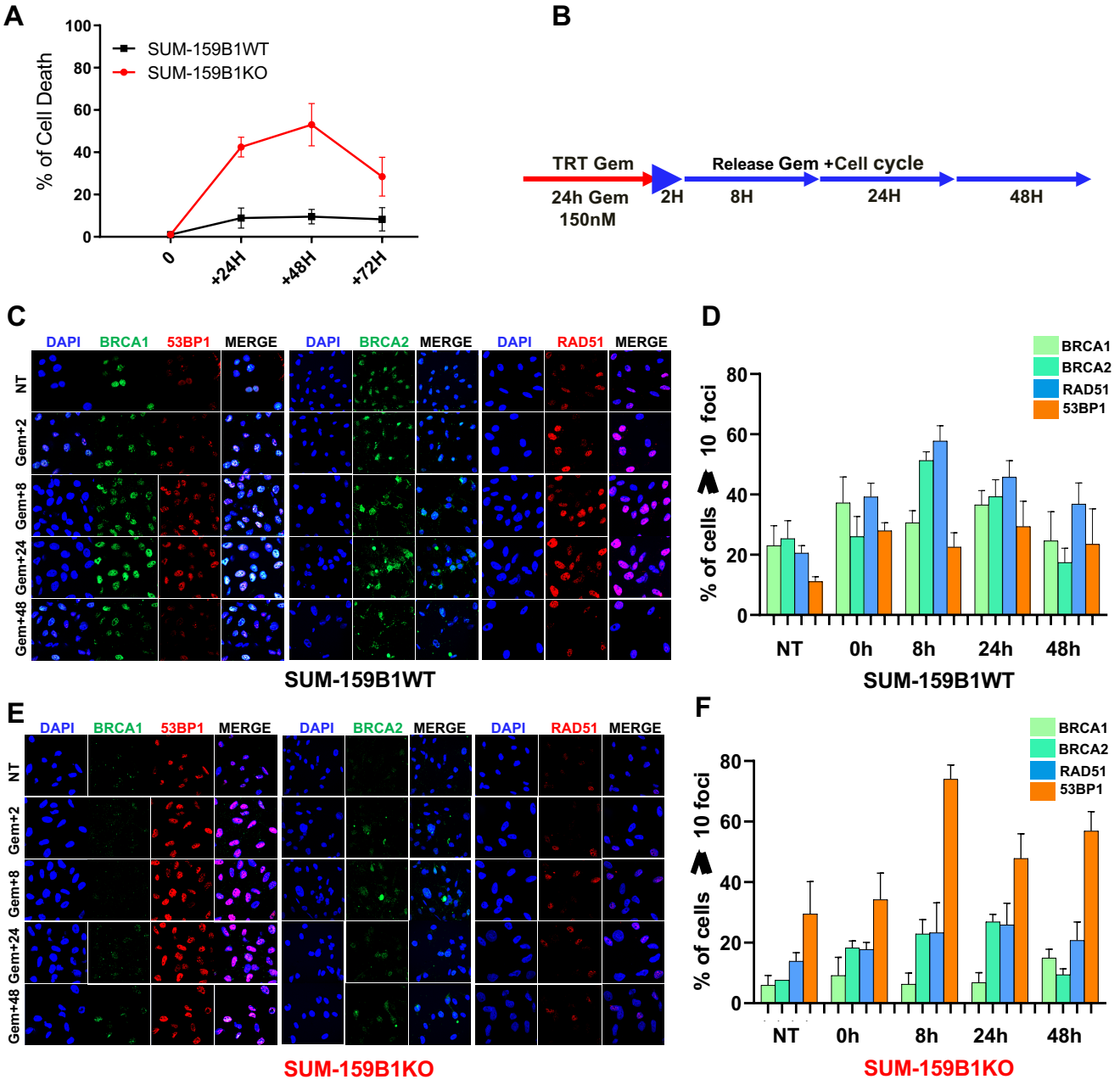

Figure 1: BRCA1-deficiency is associated with accrued gemcitabine mortality and absence of HR response A: mortality graphs of gemcitabine treated SUM159B1WT (black) and SUM159B1KO (red) cells. Cell death was assessed by FACS quantification and combines AnnexinV+ and propidium iodide+ cells. **B:** treatment protocol applied here; cells were exposed to the drug for 24h, then left to recover in fresh medium for 48h before mortality was measured. **C, D**: immunofluorescence analysis and quantification of BRCA1, BRCA2, RAD51 and 53BP1 nuclear foci formation in SUM-159B1WT cells upon gemcitabine treatment. **E, F:** same as C, D but with SUM-159B1KO cells. Cells presenting more than 10 nuclear foci by immunofluorescence were scored positive and at least 300 cells were scored per slide.

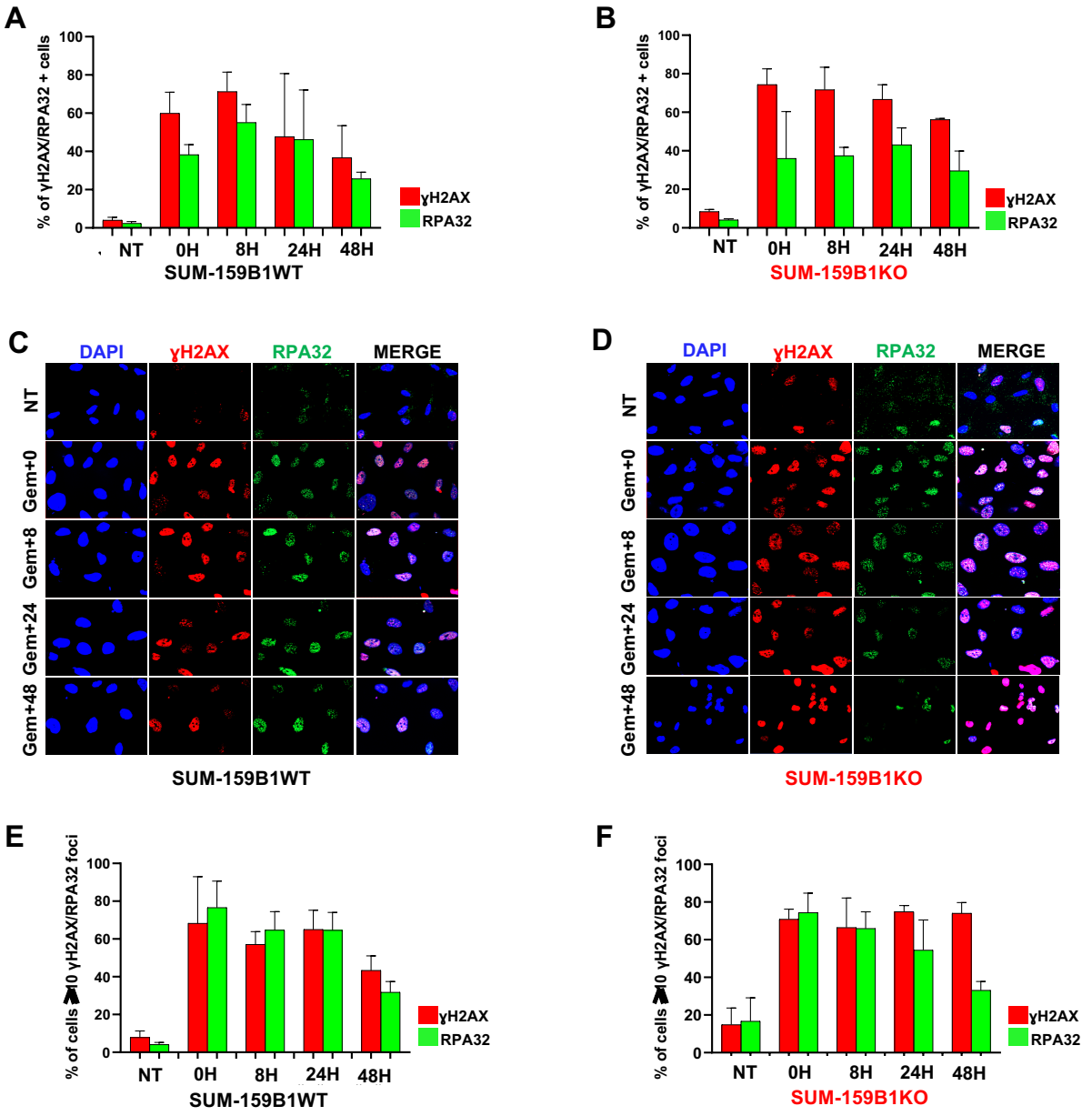

Figure 2: Gemcitabine treatment induces severe and persitent replication stress in BRCA1-deficient cell models. A, B: FACS analysis quantification of γH2AX-positive and RPA-positive cell fractions in SUM-159B1 (A) and SUM-159B1KO (B), note the imbalance between γH2AX and RPA. **C, D:** the γH2AX/RPA imbalance was also noticeable by immunofluorescence. selected sets of immunofluorescence sections of SUM-159B1WT (C) and SUM-159B1KO (D) stained with anti-γH2AX (red) and RPA (green) antibodies **E, F:** quantification of γH2AX-positive and RPA-positive cells by IF, at least 300 cells were scored by slide.

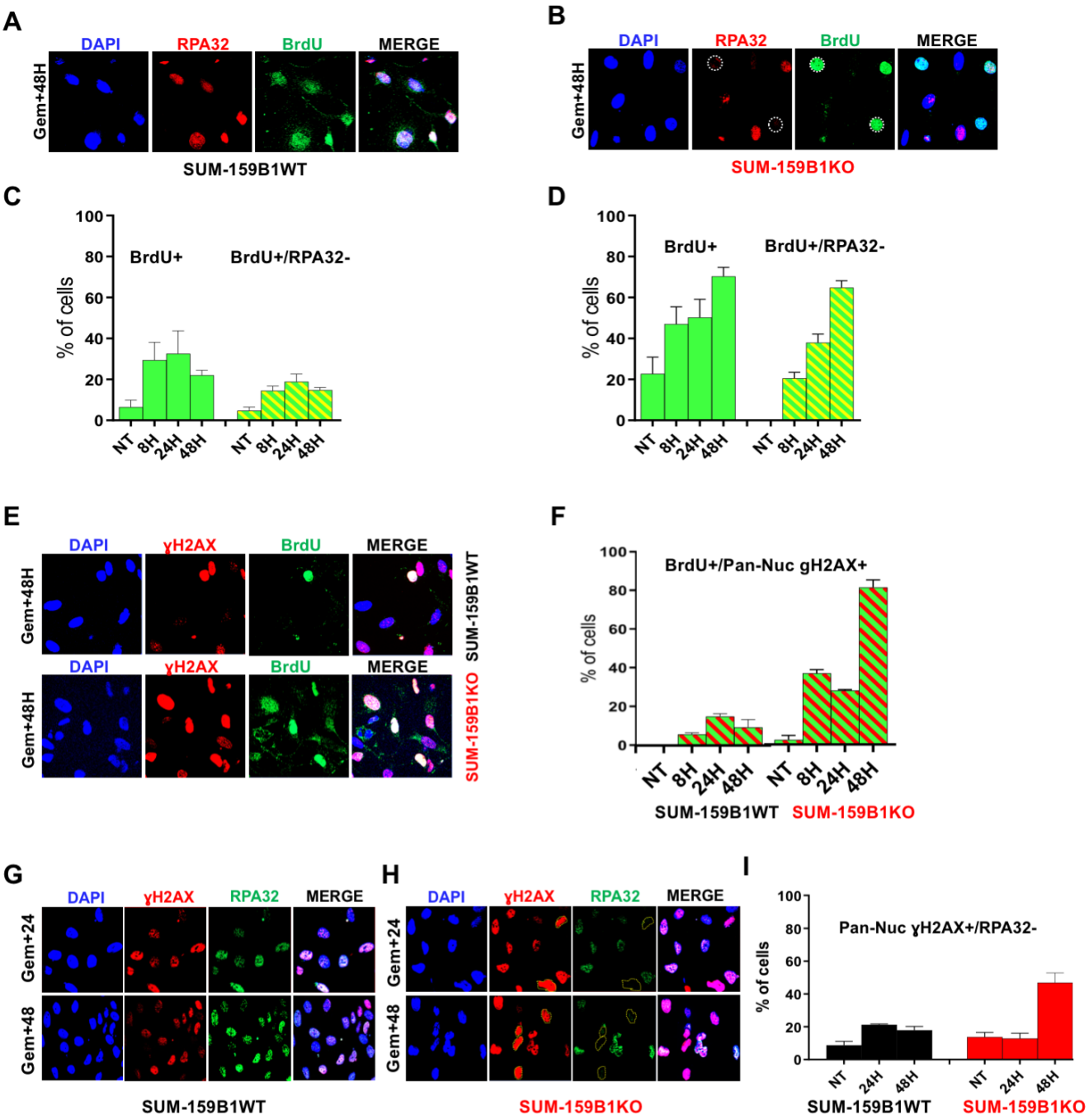

Figure 3: cells undergoing replication catastrophe are characterized by an intense BrdU, absence of RPA signal and pan-nuclear γH2AX staining. A, B: examples and quantification of RPA and BrdU immunofluorescence staining in SUM-159B1WT and SUM-159B1KO. Yellow circles in B indicate cells showing no RPA signal and intense BrdU staining **C, D**: γH2AX, BrdU and RPA32 staining patterns 48h after drug removal in SUM-159B1WT and SUM-159B1KO. Yellow circles in D indicate cells showing no or low RPA signal and a strong pan-nuclear γH2AX staining. **E**: quantification of the fraction of BrdU+ cells with pan-nuclear γH2AX staining in SUM-159B1WT and SUM-159B1KO. **F**: quantification of the fraction of pan-nuclear γH2AX staining cells showing no RPA32 signal in SUM-159B1WT and SUM-159B1KO.

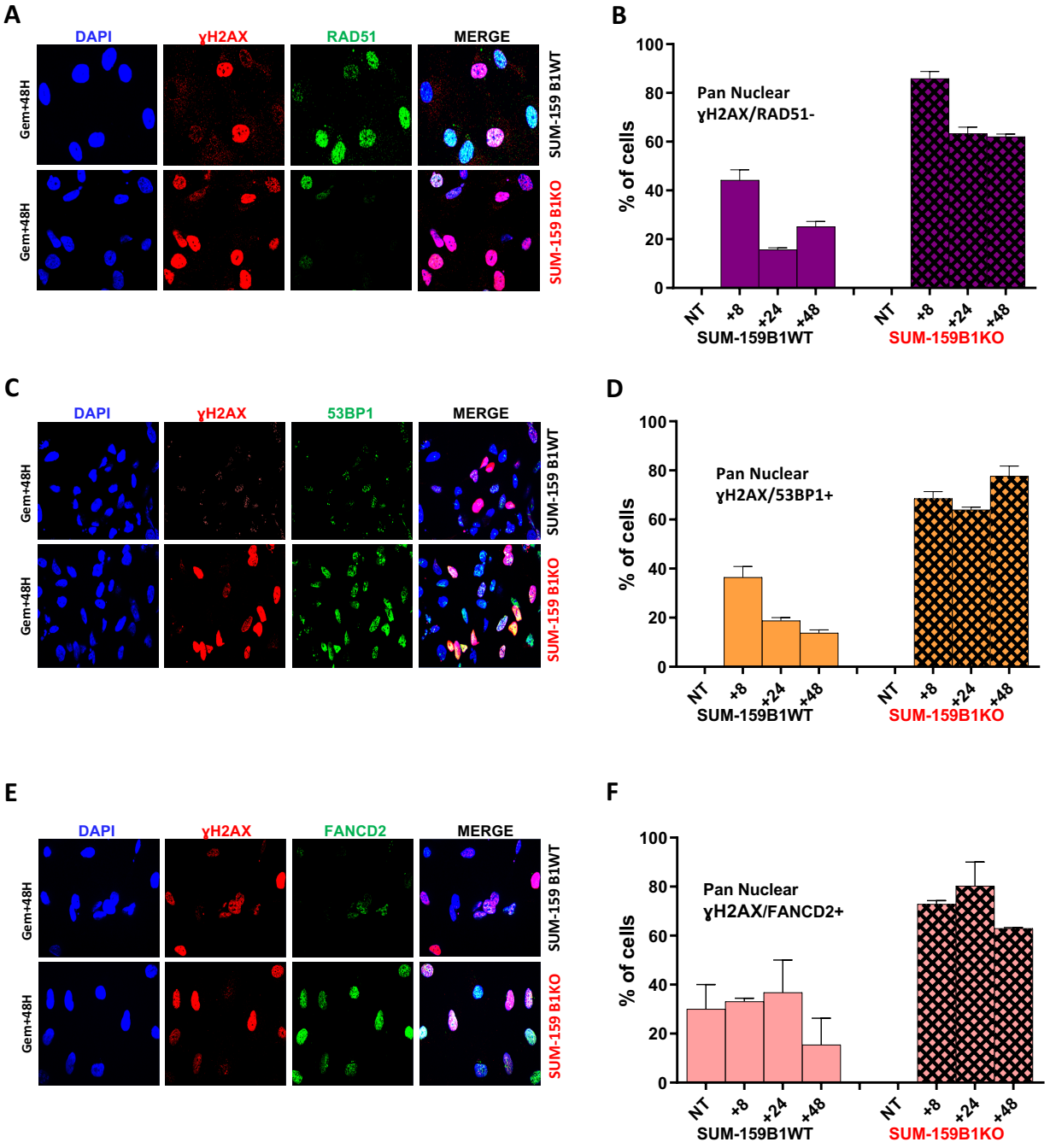

Figure 4: cells with pan-nuclear γH2AX staining show no RAD51 foci, but strong 53BP1 and FANCD2 signals. A, B: examples of γH2AX and RAD51 immunofluorescence staining 48H after drug removal and quantification of pan-nuclear γH2AX+/RAD51- cells in SUM-159B1WT and SUM-159B1KO I. **C, D:** examples of γH2AX and 53BP1 immunostaining and quantification of pan-nuclear γH2AX+/53BP1+ cells in SUM-159B1WT and SUM-159B1KO. **E, F:** examples of γH2AX and FANCD2 immunostaining and quantification of pan-nuclear γH2AX+/FANCD2+ cells in SUM-159B1WT and SUM-159B1KO

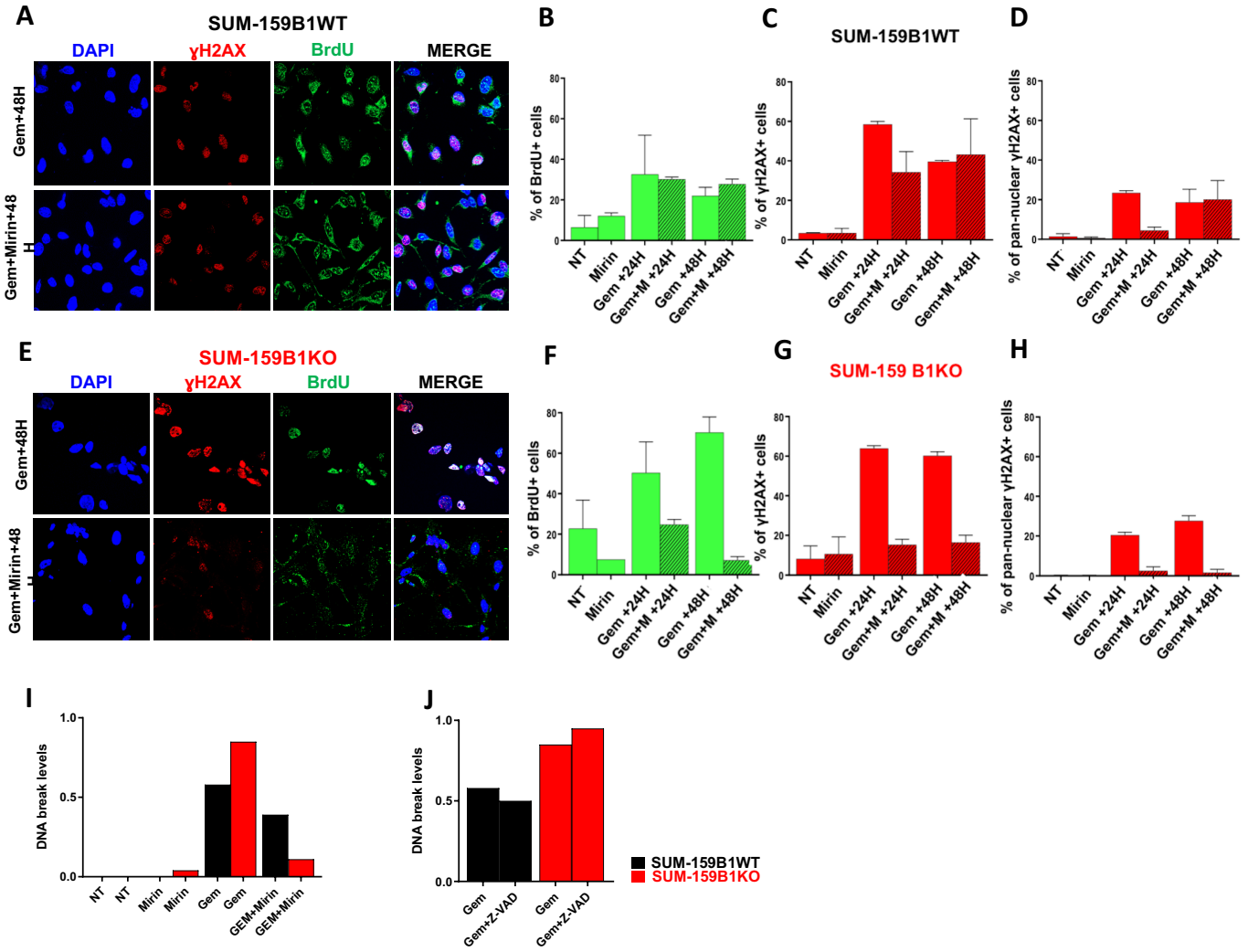

Figure 5: MRE11 is instrumental for ssDNA accumulation and onset of replication catastrophe in gemcitabine treated BRCA1-deficient cells. A, B, C, D: impact of Mirin treatment on the number of BrdU and γH2AX positive cells in gemcitabine treated SUM-159B1WT. γH2AX and BrdU immunofluorescence staining in cells treated with Gemcitabine (top row) and Gemcitabine + mirin (bottom row) (A). Quantification of BrdU+ cells in the different conditions (B). Quantification of γH2AX+ cells (C). Quantification of cells with pan-nuclear γH2AX staining (D). **E, F, G, H:** impact of Mirin treatment on the number of BrdU and γH2AX positive cells in gemcitabine treated SUM-159B1KO. γH2AX and BrdU immunofluorescence staining in cells treated with Gemcitabine (top row) and Gemcitabine + mirin (bottom row) (E). Quantification of BrdU+ cells in the different conditions (F). Quantification of γH2AX+ cells (G). Quantification of cells with pan-nuclear γH2AX staining (H). **I:** quantification of DSB breaks in SUM-159B1WT (black bars) and SUM-159B1KO (red bars) treated with gemcitabine +/- mirin. **J:** quantification of DSB breaks in SUM-159B1WT and SUM-159B1KO treated with gemcitabine +/- Z-VAD.

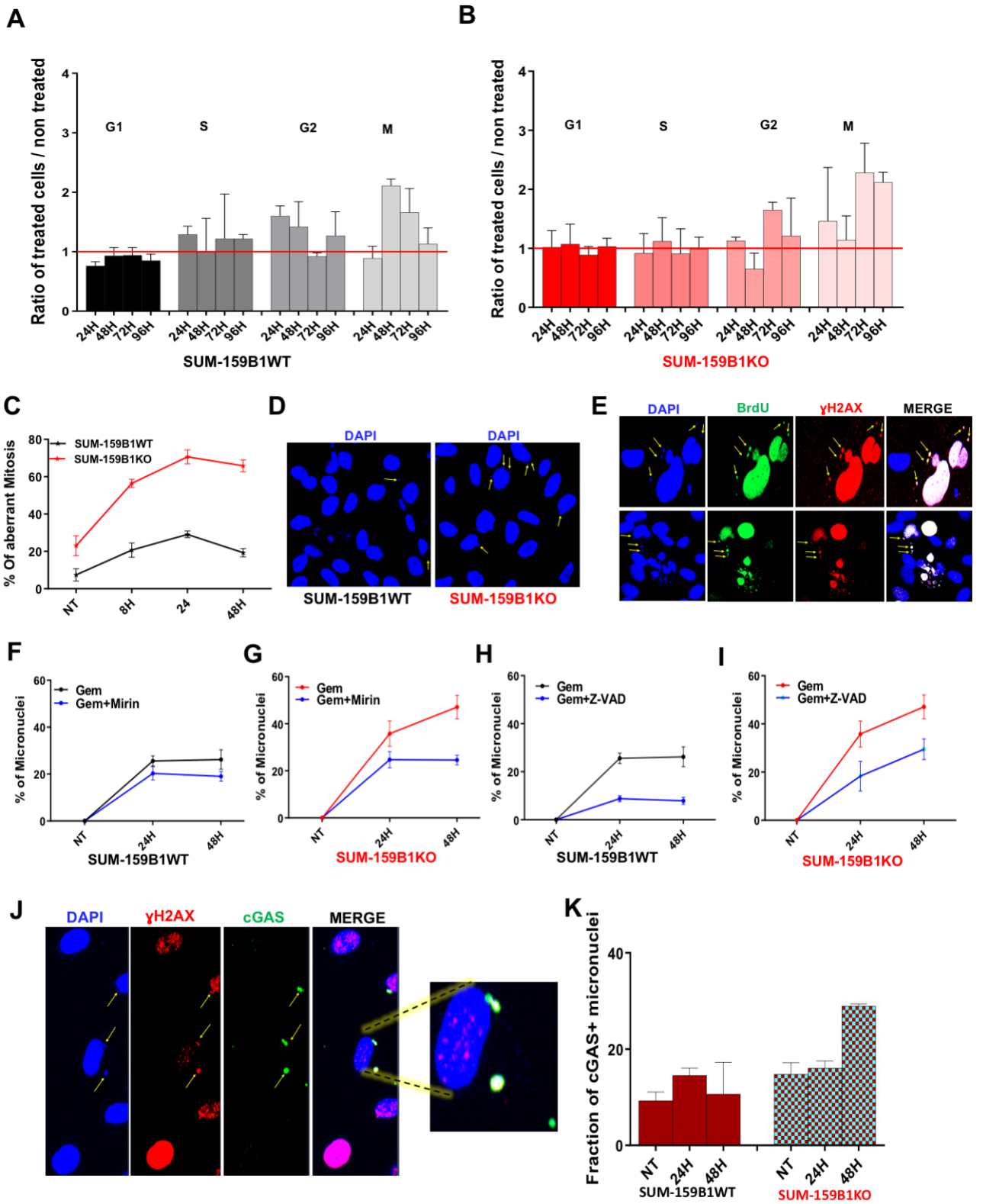

Figure 6: replication catastrophe BRCA1-deficient cells produce aberrant mitoses and trigger cGAS-STING response. **A, B:** cell cycle changes in synchronized SUM-159B1WT and SUM-159KO cells. Results present the ratio Treated/Nontreated cells. **C**: fraction of aberrant mitoses in gemcitabine treated cells. Red SUM-159B1KO, black SUM-159B1WT. **D:** micronuclei formation in gemcitabine treated SUM-159B1WT and SUM-159KO cells. **E:** in SUM-159KO micronuclei are BrdU and γH2AX positive. **F, G:** impact of mirin treatment on micronuclei numbers. **H, I:** impact of Z-VADFMK treatment on micronuclei numbers. **J, K**: γH2AX+ micronuclei show cGAS staining.